

THE SCHEME OF ANTINEUTRINO SOURCE WITH REGULATED HARD SPECTRUM ON THE BASE OF NUCLEAR REACTOR AND POSSIBLE EXPERIMENT FOR SEARCH OF STERILE NEUTRINOS

V. I. Lyashuk^{1, 2, §}

¹ *Institute for Nuclear Researches of the Russian Academy of Sciences, Moscow, Russia*

² *National Research Center "Kurchatov Institute", Moscow, Russia*

Abstract: The new principle of $\bar{\nu}_e$ -source for future short-baseline experiments is considered. The scheme is based on ${}^7\text{Li}(n,\gamma){}^8\text{Li}$ activation near the reactor active zone (AZ) and transport of the fast β^- -decaying ${}^8\text{Li}$ ($T_{1/2}({}^8\text{Li}) = 0.84$ s) toward a remote neutrino detector and back in the closed loop to AZ for the next (n,γ) -activation of lithium in the continuous cycle. The scheme with closed loop ensures well defined total spectrum (in the position of the neutrino detector) that will allow to decrease the count errors below $\lesssim 1\%$. Owing to $\sigma \sim E_\nu^2$ dependence of neutrino cross section the count rate will be more than $\sim 10^3$ per day for the compact detector with volume about m^3 . The proposed experiment allows to detect $(\bar{\nu}_e, p)$ -interaction with high precision and directed to search of sterile neutrinos with $\Delta m^2 \sim 1$ eV^2 . Basing on the proposed algorithm it were indicated the space regions for search of $\bar{\nu}_e$ -disappearance for (3+1) and (3+2) neutrino models in the discussed experiment with new hard spectrum intensive $\bar{\nu}_e$ -source.

1. INTRODUCTION. NUCLEAR REACTOR AS ANTINEUTRINO SOURCE: THE ADVANTAGES FOR THE EXPERIMENT AND PROBLEMS OF ITS SPECTRUM

The undoubted advance in solution of the discussed problem (search of sterile neutrinos) is creation of the intensive antineutrino source with well-known hard spectrum. The most intensive artificial antineutrino sources used for neutrino experiments are the nuclear reactors. The resulting reactor antineutrino flux is the complicated additive function of fluxes: from fission fragments; from beta decay of heavy (transuranium) nuclei (produced in (n,γ) - and $(n,2n)$ -reactions); and β -decay of (n,γ) -activated elements of the constructions and water. In spite of the doubtless superiority in flux value the antineutrino reactor spectra (formed by main fuel isotopes – ${}^{235}\text{U}$, ${}^{238}\text{U}$, ${}^{239}\text{Pu}$, ${}^{241}\text{Pu}$) are characterized by large uncertainties in the total $\bar{\nu}_e$ -spectrum that lead to very serious problems in interpretation of neutrino oscillation results. The reactor spectrum is known with $\sim (4-6)\%$ -precision at energy up to ~ 6 MeV and these errors dramatically rise up to tens percent at more higher energies (see spectrum errors in Fig. 1) [1–4].

An equilibrium $\bar{\nu}_e$ -spectrum of nucleus-fission products from nuclear fuel composition varies in time in operation period and in case of reactor stops: the isotope ${}^{235}\text{U}$ burns away (it's part in number of fissions decrease in operation period from $\sim 73\%$ down to 45%), but the contributions of ${}^{238}\text{U}$, ${}^{239}\text{Pu}$ and ${}^{241}\text{Pu}$ rise (so, for ${}^{239}\text{Pu}$ the yield to fissions increases from 18% up to 37% for the same time). The large changing in composition leads to variation in $\bar{\nu}_e$ -fluxes which are recalculated by means of correction factors for four main fuel isotopes.

[§] lyashuk@itep.ru

The all spectra drop rapidly as energy increases (that is especially negatively for registration of threshold $\bar{\nu}_e$ -reactions): at increase $E_{\bar{\nu}}$ from 2 MeV to 4, 6 and 8 MeV the neutrino spectrum of ^{235}U drops in 5, 35 and 956 times, correspondingly (example in Fig. 1 for spectrum from ^{235}U).

An additional unaccounted error for $\bar{\nu}_e$ -flux evaluation appears during reactor stops due to permanent presence of cooling pond for spent fuel. These errors can rise up to 1%. The summary neutrino flux depends on number of fissions in the active zone as: $n_f(t) = W(t)/E_f(t)$, where $W(t)$ is a full reactor heat power for the current time and E_f is the mean energy released per one fission. But the E_f value is also changing during the reactor life time: it increasing on 1.5% [3].

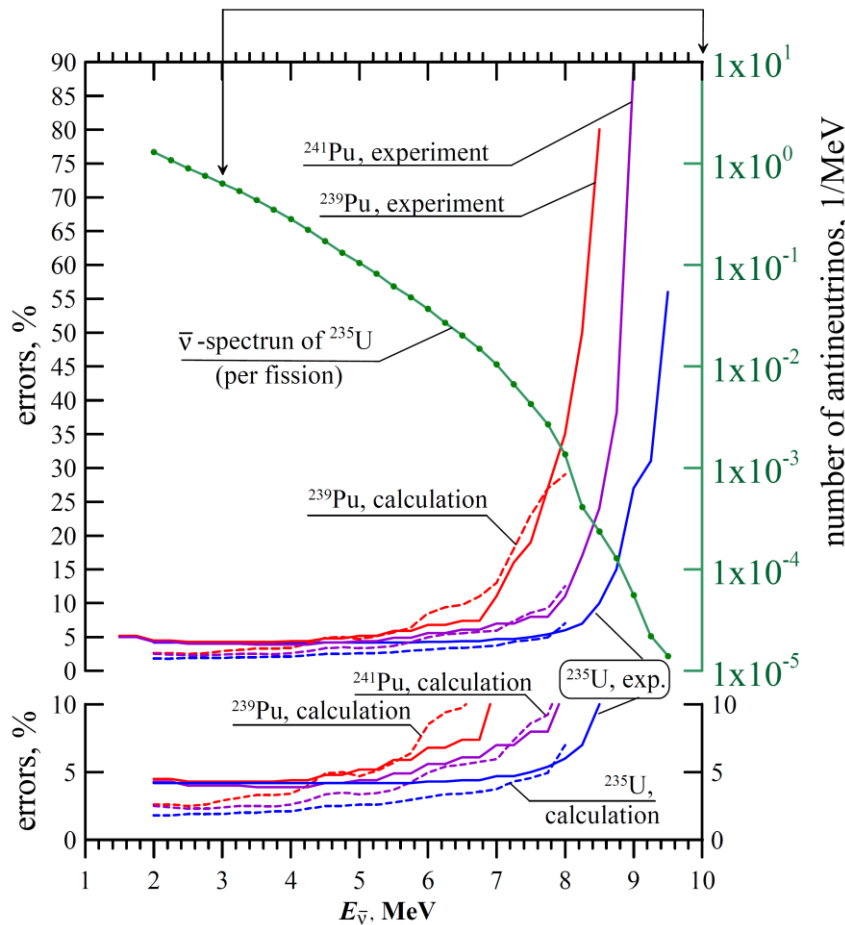


Fig.1. Dependence of antineutrino spectrum errors from energy for $\bar{\nu}_e$ -spectrum of fission products of ^{235}U , ^{239}Pu and ^{241}Pu (see left vertical axes); the results presented in two scales of errors for experimental data (solid lines [1]) and calculations (dotted lines [2]). Antineutrino spectrum of ^{235}U is shown by solid line with point (see right vertical axis [2]) on the top part.

In the recent measurements of $\bar{\nu}_e$ -spectrum in Daya Bay, Reno and Double Chooz experiments it was detected significant excess of antineutrinos in the interval $\sim (5-7)$ MeV of the spectrum [5-7]. This excess in experimental spectrum (called as bump) was unexpected and significantly activated efforts in order to clarify the matter. Here we want to emphasize that the requirement of well definite antineutrino spectrum of the source is exclusively important for excluding of the possible errors in the proposed experiment (see below) for search of sterile neutrinos.

2. PROPOSED HIGH FLUX $\bar{\nu}_e$ -SOURCE OF HARD REGULATED SPECTRUM

In spite of the apparent superiority on neutrino flux the nuclear reactors has a

disadvantage: too-small hardness of $\bar{\nu}_e$ -spectrum. This character is extremely negative as the probability of registration strongly depends on neutrino energy. For the considered here reactor antineutrino energy the neutrino cross section is proportional to its energy squared ($\sigma_\nu \sim E_\nu^2$). In case of hard ${}^8\text{Li}$ spectrum the square-law dependence results in strong rise of neutrino cross section. The disadvantage of rapidly dropping reactor spectrum can be filled having realized the idea [8] to use a high-purified isotope ${}^7\text{Li}$ for construction of lithium blanket (or converter) around the active zone (AZ) of a reactor. A short-lived isotope ${}^8\text{Li}$ ($T_{1/2} = 0.84$ s) is created under AZ neutrons flux in reaction ${}^7\text{Li}(n,\gamma){}^8\text{Li}$ and at β^- -decay it emits hard antineutrinos of a well determined spectrum with the maximal energy $E_{\bar{\nu}}^{\max} \approx 13.0$ MeV and mean one $\bar{E}_{\bar{\nu}} \approx 6.5$ MeV.

The scheme of β^- -decay of ${}^8\text{Li}$ (with $\sim 100\%$ branching) to broad 3.03 MeV level of ${}^8\text{Be}^*$ (first-excited state of ${}^8\text{Be}$; $\Gamma \approx 1.513$ MeV) and then to two alpha-particles is presented in Fig.2 [9]. The β^- -decay of ${}^8\text{Li}$ is a pure Gamov-Teller ($\Delta T = 1$) transition.

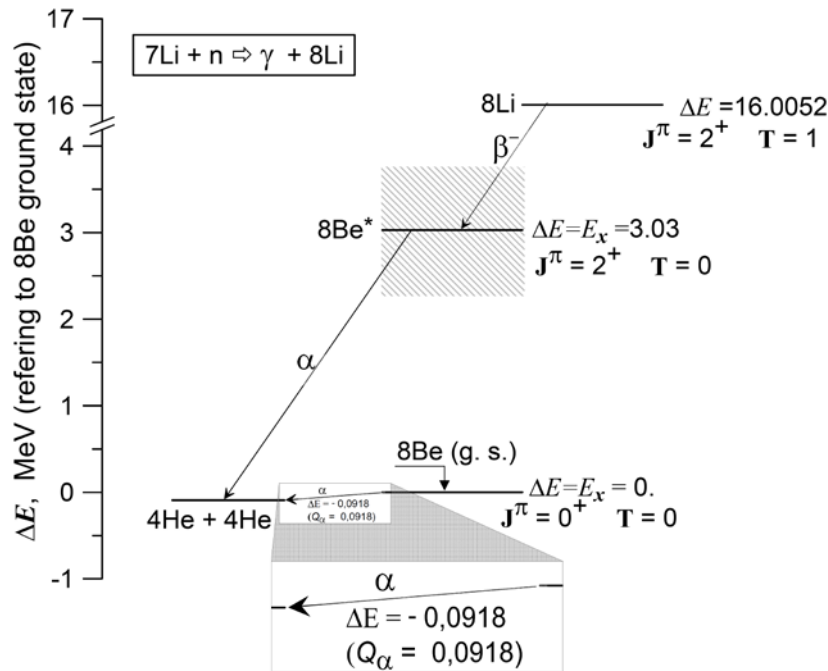


Fig. 2. The scheme of β^- -decay for ${}^8\text{Li}$ with delayed α -decay. The indicated energies ΔE (shown right to the levels) are given refer to the ground state (g.s.) level of ${}^8\text{Be}$ ($J^\pi = 0^+$, $T = 0$). The broad 3.03 MeV level of ${}^8\text{Be}^*$ is shown by shading ($\Gamma \approx 1.513$ MeV). J – the angular momentum; π – parity; and T – isobaric spin; E_x – excited level of ${}^8\text{Be}$; Q_α – energy of α -decay. The α -decay of ${}^8\text{Be}(\text{g.s.}) \rightarrow {}^4\text{He} + {}^4\text{He}$ is shown by means the magnification software.

The resulting antineutrino flux from such a source (AZ plus ${}^7\text{Li}$ blanket-converter) will be total one (produced by β^- -decay of ${}^8\text{Li}$ and from AZ). The problem of creation of intensive antineutrino source with well definite hard spectrum can be solved by the scheme of (n,γ) -activated ${}^7\text{Li}$ isotope (irradiated by reactor neutrons close the AZ as lithium blanket) and continuous circulation of lithium isotope (or liquid lithium substance) in the close loop from AZ to remote neutrino detector [10–16]. The most perspective lithium substance can be

heavy water solution of lithium hydroxides ${}^7\text{LiOD}$ or ${}^7\text{LiOD}\cdot\text{D}_2\text{O}$ [16, 19]. With purpose to increase the hard lithium antineutrino part (in the total antineutrino spectrum) we propose to construct the volumable pumped reservoir close to the antineutrino detector.

The scheme for this type of the dynamical (with pumped lithium) $\bar{\nu}_e$ -source is presented in Fig.3 [15, 16]. Namely this scheme (with specified dimensions) was used in the discussed below simulation for search of sterile neutrinos.

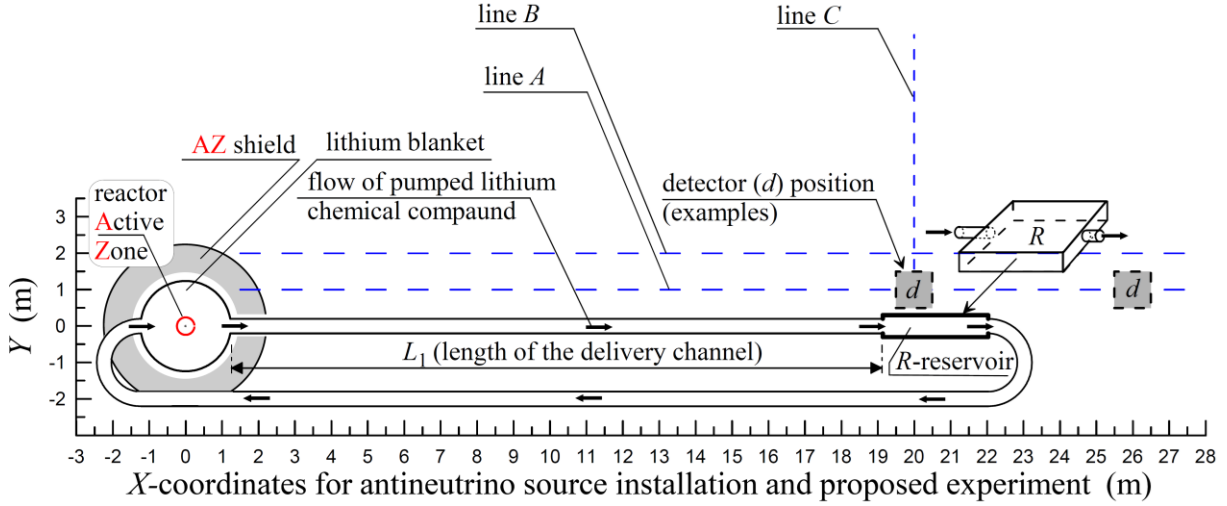


Fig. 3. The conceptual scheme of $\bar{\nu}_e$ -source (with circulation of ${}^8\text{Li}$ or lithium chemical substance in the closed loop) with variable (regulated and controlled) spectrum for short base line experiment. The distribution of the total antineutrino spectrum is regulated by the rate of lithium pumping (which can be smoothly varied by means the pump in the installation). The all dimensions in the scheme fully correspond to sizes used in the simulation of the experiment. Lithium substance in the blanket (activated by AZ-neutrons) is pumped continuously through the delivery channel to the remote reservoir (volume which is set close to the $\bar{\nu}_e$ -detector) and further back to the blanket. The examples of detector positions are labelled as "d". The 3-dimensional view of the reservoir (labeled by "R") is given separately. At simulation of the antineutrino disappearance (see below) we used the coordinates of points along lines: A ($y = 1$), B ($y = 2$) and C ($x = 20$).

For our purpose (creation of the neutrino source of significantly larger hardness than possible to obtain by above mentioned simple scheme of lithium blanket around the AZ) we introduce the definition of the generalized hardness for total neutrino spectrum [15, 16]. Let $F_{\text{Li}}(\vec{r})$ and $F_{\text{AZ}}(\vec{r})$ – densities of lithium $\bar{\nu}_e$ -fluxes from the blanket and from AZ, $\bar{n}_\nu \approx 6.14$ is number of reactor antineutrinos emitted per one fission in the AZ. We admit that the hardness of the summary $\bar{\nu}_e$ - spectrum at the point \vec{r} equals one unit of hardness if the ratio of densities $F_{\text{Li}}(\vec{r})/F_{\text{AZ}}(\vec{r})$ equals to $1/\bar{n}_\nu$. Let us define the total spectrum generalized hardness as:

$$H(\vec{r}) = \bar{n}_\nu \frac{F_{\text{Li}}(\vec{r})}{F_{\text{AZ}}(\vec{r})} . \quad (1)$$

In the simulation we specified the next parameters of the source and regime of the operation. Volume of the compact spherical AZ corresponds to 51 liters volume of the high flux research reactor PIK near the Saint-Petersburg in Russia [20, 21]. Thickness of the spherical lithium blanket is 1 m. Volume of the reservoir (rectangular parallelepiped of 0.5 m thickness) was set equal to blanket one. L_1 is a distance between lithium blanket and pumped reservoir. In the simulation the volume rate of pumping was $w = 2.25 \text{ m}^3/\text{s}$. The distance L_1 corresponds to the time 1 s of lithium delivery from the blanket to reservoir for appointed w rate.

3. POSSIBLE EXPERIMENT FOR SEARCH OF STERILE NEUTRINOS

In some realized oscillation experiments (LSND [22], SAGE [23], MiniBooNe [24, 25], GALLEX [26], reactor experiments [27]) it were revealed anomalous $\bar{\nu}_e$ -fluxes and strongly stimulated the discussion on existence of sterile neutrinos and extension of the Standard Model. The discussed variants include models with one, two and three type of sterile neutrinos [28–32]. Some results indicate on the squared-mass difference between sterile and active neutrinos ($\Delta m^2 \sim 1 \text{ eV}^2$).

The discussed here short base line experiment on sterile neutrino search (in the geometry of Fig. 3) has advantages namely at short distances where the large hardness is ensured. For short base line geometry in case of (3+1)-model (i.e., three active neutrinos plus one sterile) the probability of existence at distance L is given by means two-flavor model:

$$P = 1 - \sin^2(2\theta)\sin^2[1.27\Delta m_{41}^2(L(\text{m})/E(\text{MeV}))], \quad (2)$$

$$\sin^2(2\theta) = 4|U_{i4}|^2(1 - |U_{i4}|^2), \quad (3)$$

where θ – angle of mixing, Δm_{41}^2 (eV^2) – maximum squared-mass difference between sterile and active neutrinos (i.e., $|\Delta m_{41}^2| \gg |\Delta m_{31}^2| \gg |\Delta m_{21}^2|$), U_{i4} – element of mixing matrix for active neutrino flavor $i = e, \mu, \tau$.

Probability for (3+2)-model (i.e., three active neutrinos plus two sterile neutrinos) for short base geometry will be:

$$P_e = 1 - 4(1 - |U_{e4}|^2 - |U_{e5}|^2) \times \{|U_{e4}|^2 \sin^2[1.27\Delta m_{41}^2(L/E)] + |U_{e5}|^2 \sin^2[1.27\Delta m_{51}^2(L/E)]\} - 4 |U_{e4}|^2 |U_{e5}|^2 \sin^2[1.27\Delta m_{54}^2(L/E)]. \quad (4)$$

For simulation of the probability of $\bar{\nu}_e$ -existence, fluxes and expected ($\bar{\nu}_e, p$)-events in the detector the full volume of the source (i.e., AZ, lithium blanket, channels and reservoir in the Fig. 3) was divided on small cell. The obtained equations of ${}^8\text{Li}$ production depending on the parameters of the source scheme (the geometry, yield of ${}^8\text{Li}$, the pumping regime (see details of calculations in [15–16]) allows to calculate the number of ${}^8\text{Li}$ nuclei in any cells for the given geometry and pumping regime. It allows to calculate the flux, spectrum, hardness at the detector positions (for the specified AZ power). The highest level of hardness (that is important for high rate of counts and low errors) is supported in the closed space around the voluminous reservoir. For analysis of oscillation we considered the next simple realistic geometry: the detector (or detectors) can be set and shifted along the line A, B or C (Fig. 3). This detector geometry is realistic owing to high count rate in the hard spectrum and possibility to reduce the sensitive volume up to $\sim \text{m}^3$ (see below). For AZ spectrum it was taken that the single fuel element is ${}^{235}\text{U}$ similar to reactor PIK [20, 21]. The density of $\bar{\nu}_e$ -flux from AZ is determined by its power P and for distance R is:

$$F (\text{cm}^{-2} \cdot \text{s}^{-1}) = \bar{n}_\nu P / 4\pi R^2 \bar{E} \approx 1.5 \times 10^{12} P (\text{MW}) / R^2 (\text{m}), \quad (5)$$

where $\bar{E} \approx 200 \text{ MeV}$ - mean energy released at ^{235}U -fission.

In the calculation the applied proton concentration in the detector is typical – about $6.6 \times 10^{22} \text{ cm}^{-3}$ (KamLAND liquid scintillator [33]). The matrix elements for (3+1) and (3+2)-models correspond to best fits of the work [28]: for (3+1) model – $\Delta m_{41}^2 = 1.78 \text{ eV}^2$, $U_{e4} = 0.151$; for (3+2)a-model – $\Delta m_{41}^2 = 0.46 \text{ eV}^2$, $U_{e4} = 0.108$, $\Delta m_{51}^2 = 0.89 \text{ eV}^2$, $U_{e5} = 0.124$; for (3+2)b-model – $\Delta m_{41}^2 = 0.47 \text{ eV}^2$, $U_{e4} = 0.128$, $\Delta m_{51}^2 = 0.87 \text{ eV}^2$, $U_{e5} = 0.138$. The update analysis of last neutrino experiments gives (some differing global-fit-parameters for sterile neutrinos with $\Delta m^2 \sim 1 \text{ eV}^2$ was obtained in the [34]).

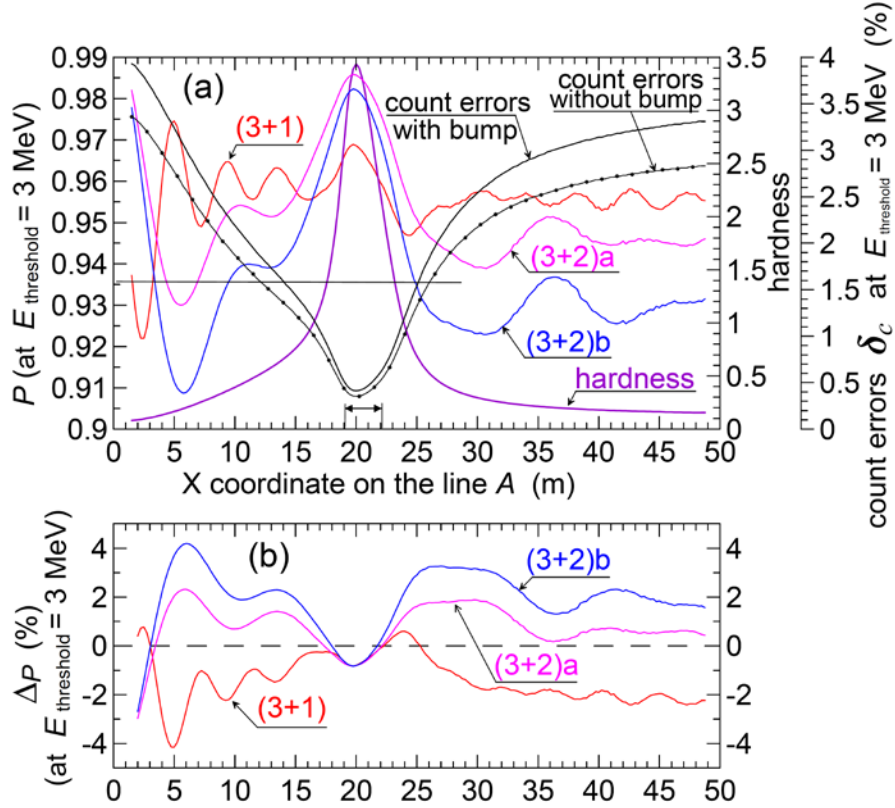


Fig.4. Probability P of $\bar{\nu}_e$ -existence for three models [(3+1), (3+2)a and (3+2)b on the part (a)], hardness H of the total $\bar{\nu}_e$ -spectrum [part (a)], count errors δ_C (caused by uncertainties of AZ spectrum) [part (a)] and functional $\Delta_P(x)$ for opportunity of $\bar{\nu}_e$ -detecting [part (b)] for models: (3+1), (3+2)a and (3+2)b] depending on the X coordinate **along the line A** (for the detector geometry of Fig. 3). Probability P , count errors δ_C and functional Δ_P are presented for the threshold of registration $E = 3 \text{ MeV}$. The all solid lines correspond the values obtained for $\bar{\nu}_e$ -spectrum with reactor bump taken into account. The curves with points [count errors δ_C in the parts (a)] – the errors of $\bar{\nu}_e$ -counts for reactor spectrum without bump. Position of the reservoir is shown by the two-sided arrow on the part (a). X coordinates of the positive Δ_P values are the regions where probability of $\bar{\nu}_e$ -detecting is higher to level of total spectrum errors (see part (b)).

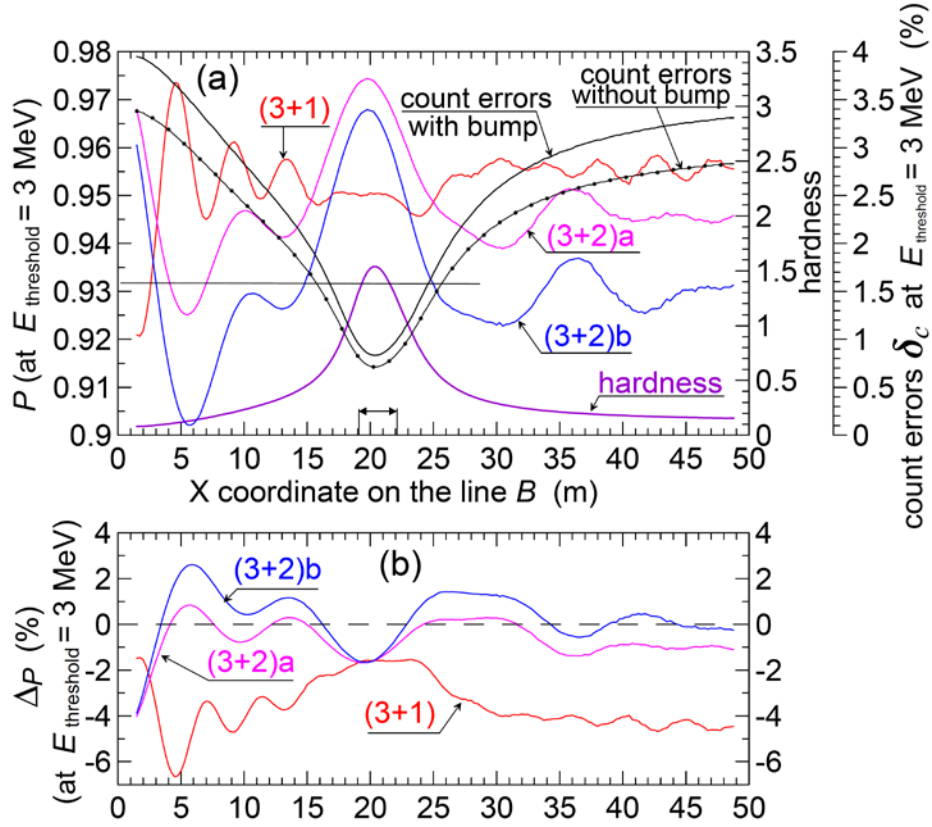


Fig.5. Probability P of $\bar{\nu}_e$ -existence for three models [(3+1), (3+2)a and (3+2)b on the part (a)], hardness H of the total $\bar{\nu}_e$ -spectrum [part (a)], count errors δ_C (caused by uncertainties of AZ spectrum) [part (a)] and functional $\Delta_P(x)$ for opportunity of $\bar{\nu}_e$ -detecting [part (b)] for models: (3+1), (3+2)a and (3+2)b] depending on the X coordinate **along the line B** (for the detector geometry of Fig. 3). Probability P , count errors δ_C and functional Δ_P are presented for the threshold of registration $E = 3 \text{ MeV}$. The all solid lines correspond the values obtained for $\bar{\nu}_e$ -spectrum with reactor bump taken into account. The curves with points [count errors δ_C in the parts (a)] – the errors of $\bar{\nu}_e$ -counts for reactor spectrum without bump. Position of the reservoir is shown by the two-sided arrow on the part (a). X coordinates of the positive Δ_P values are the regions where probability of $\bar{\nu}_e$ -detecting is higher to level of total spectrum errors (see part (b)).

The calculated errors for count events are given here at 100% efficiency of registration. Fig. 4(a) shows the probability P of existence, hardness and count errors for models (3+1), (3+2)a and (3+2)b at the antineutrino registration threshold $E_{\text{threshold}} = 3 \text{ MeV}$ for detector positions along lines A (see Fig. 3). Note that hardness H does not depend on the threshold on registration [according to definition (1)]. Fig. 5(a) presents the same values for detector positions along line B (see Fig. 3). Fig. 6(a) shows the above mentioned values for orthogonal line C (see Fig. 3). At coordinates of the reservoir the hardness reaches the maximum with small shift to AZ-position due to decrease of ^8Li concentration along the flow (see Fig. 4(a) and 5(a)). Owing to large lithium mass in the reservoir the maximum of probability P is detected close to its position (marked by double arrow) in Figs. 4(a) and 5(a). Large hardness

around the reservoir ensure smallest count errors (below 0.5–1.0%) in the nearby space; shift from line *A* to line *B* leads to fall of hardness and increase of errors (compare the Fig. 4(a) and 5(a)). The most rapid decrease of hardness and rise of errors take place for line *C* - at the remote from lithium mass (see Fig. 6(a)).

In the next step we introduce the functional for possibility (or opportunity) to detect the oscillation of active to sterile neutrinos. The functional based on comparison of the maximal probability P (at the x_{fix}) with the current $P(x)$ **along A-line** ($y = 1$ m, according to the geometry in Fig. 3):

$$\Delta P(x) = [1 - \delta_C(x_{\text{fix}}, y = 1 \text{ m})] \times P(x_{\text{fix}}, y = 1 \text{ m}) - [1 + \delta_C(x, y = 1 \text{ m})] \times P(x, y = 1 \text{ m}), \quad (6)$$

where δ_C – count errors; coordinate x_{fix} corresponds to maximal P value close to reservoir: $x_{\text{fix}} \approx 20$ m. The functional helps to search change in probability P avoiding the errors caused by reactor $\bar{\nu}_e$ -spectrum. The positive ΔP values determine the X coordinate regions (along *A*-line) where probability of $\bar{\nu}_e$ -detecting is higher to level of total spectrum errors.

The $\Delta P(x)$ results are labelled as (b) and presented in the bottom parts of all Figs. 4–6 for threshold of $\bar{\nu}_e$ -registration $E_{\text{threshold}} = 3$ MeV. The analysis for detector position along the line *A* (Fig. 4) revealed that the probability to detect oscillation in case of (3+1)-model is close to zero: the $\Delta P(x)$ curves lay below zero or nearby to it. The model (3+2)a allows to reach the probability up to $\approx 2\%$, but effects for the model (3+2)b can exceed zero level by 4% (at $x \approx 6$ m, Fig. 4(b)).

The functional for possibility (to detect an oscillation to sterile neutrinos) **along B-line** ($y = 2$ m, see Fig. 3) is the similar to (6):

$$\Delta P(x) = [1 - \delta_C(x_{\text{fix}}, y = 2 \text{ m})] \times P(x_{\text{fix}}, y = 2 \text{ m}) - [1 + \delta_C(x, y = 2 \text{ m})] \times P(x, y = 2 \text{ m}). \quad (7)$$

In case of the **C-line** we compare the current probability **along the C-line** ($x = x_{\text{fix}}$) with maximal P value close to reservoir (at the coordinates: $x_{\text{fix}} \approx 20$ m, $y = 1$ m):

$$\Delta P(y) = [1 - \delta_C(x_{\text{fix}}, y = 1 \text{ m})] \times P(x_{\text{fix}}, y = 1 \text{ m}) - [1 + \delta_C(x_{\text{fix}}, y)] \times P(x_{\text{fix}}, y). \quad (8)$$

The opportunities to reveal the oscillation in the geometries along line *B* and *C* are lower (see Fig. 5(b) and 6(b)) that are explained by increased errors for lower hardness in the total spectrum.

For the discussed source the nuclear reactor acts as intensive (n, γ)-activator. The remote volumable reservoir acts as geometry factor for creation of the hard $\bar{\nu}_e$ -spectrum. As a result the proposed source ensures high neutrino flux with hard spectrum in the space close to the reservoir. Here the ^8Li isotope acts as **effective shifter** in forming of the hard spectrum. The quadratic dependence of cross section as $\sigma_{\nu} \sim E_{\nu}^2$ strongly amplifies the effect: the number of ($\bar{\nu}_e, p$)-events strongly increasing in the detector. The results of calculated counts for points on the line *A* (see detector geometry in Fig. 3) is given in the Fig. 7. Thanks to the reservoir the total flux and number of events has "lithium bump" close to the reservoir position. The number of events from ^8Li strongly dominates over the number of events from reactor antineutrinos (Fig. 7).

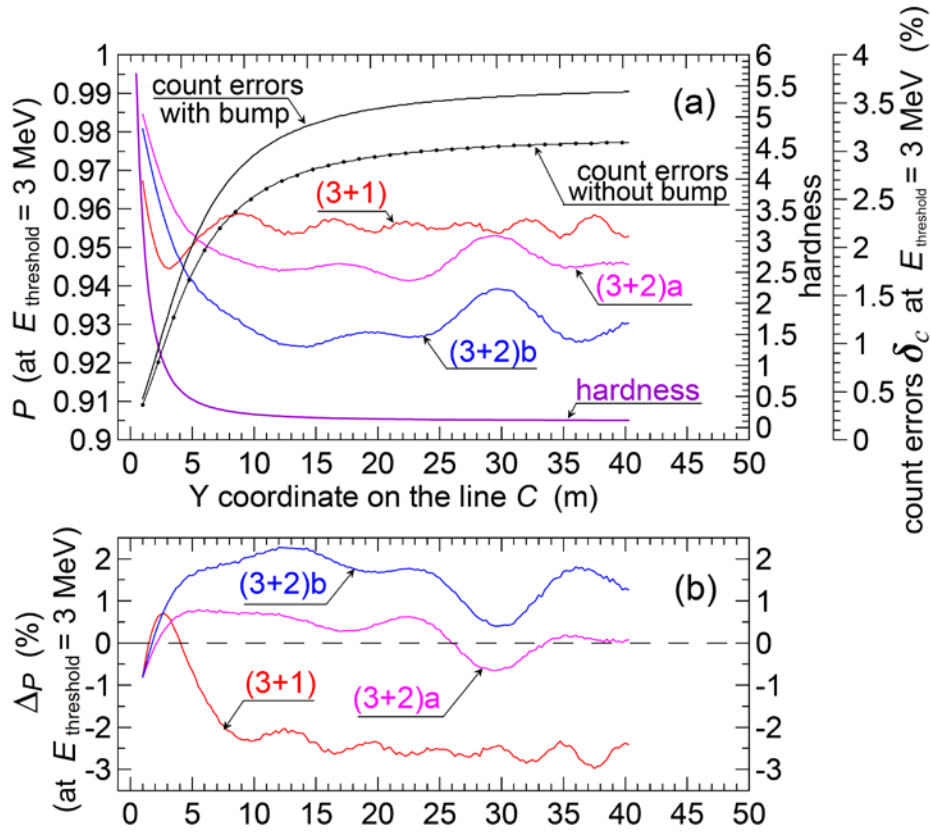


Fig.6. Probability P of $\bar{\nu}_e$ -existence for three models [(3+1), (3+2)a and (3+2)b on the part (a)], hardness H of the total $\bar{\nu}_e$ -spectrum [part (a)], count errors δ_C (caused by uncertainties of AZ spectrum) [part (a)] and functional $\Delta_P(x)$ for opportunity of $\bar{\nu}_e$ -detecting [part (b) for models: (3+1), (3+2)a and (3+2)b] depending on the X coordinate along the line C (for the detector geometry of Fig. 3). Probability P , count errors δ_C and functional Δ_P are presented for the threshold of registration $E = 3 \text{ MeV}$. The all solid lines correspond the values obtained for $\bar{\nu}_e$ -spectrum with reactor bump taken into account. The curves with points [count errors δ_C in the parts (a)] - the errors of $\bar{\nu}_e$ -counts for reactor spectrum without bump. Position of the reservoir is shown by the two-sided arrow on the part (a). X coordinates of the positive Δ_P values are the regions where probability of $\bar{\nu}_e$ -detecting is higher to level of total spectrum errors (see part (b)).

The results in Fig. 7 are normalized per cubic meter, day and gigawatt of the reactor power. We note that really the power of the investigating reactors is lower; the exclusively interesting variant (for the discussed $\bar{\nu}_e$ -source) of such reactor is new reactor PIK with the thermal power 100 MW [20–21]. The events ensured by the ${}^8\text{Li}$ antineutrinos are strongly dominates (compare to yield from AZ neutrinos) owing to the hardness of $\bar{\nu}_e$ -spectrum of ${}^8\text{Li}$.

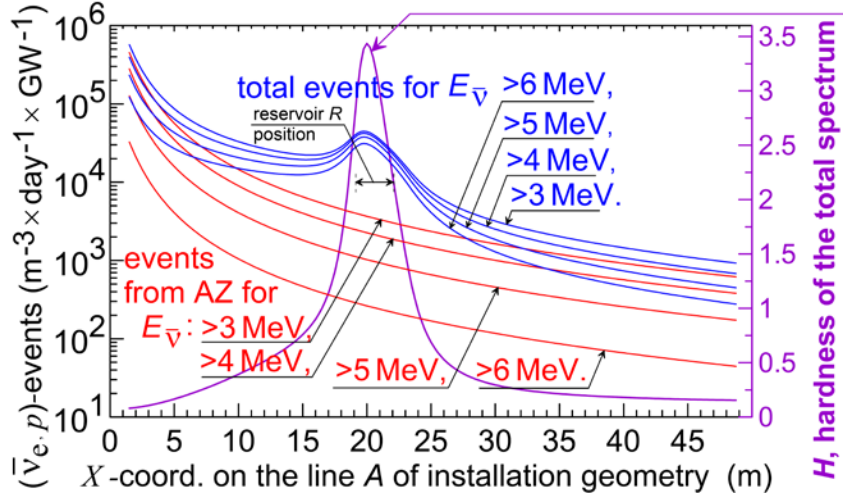


Fig. 7. The expected normalized number of $(\bar{\nu}_e, p)$ -events in the detector depending on the X coordinates along the line A (geometry of the Fig. 3). The results are given for thresholds of antineutrino registration $E_{\text{threshold}} = 3, 4, 5,$ and 6 MeV. The total number of events is ensured by $\bar{\nu}_e$ from ${}^8\text{Li}$ and AZ. Position of the reservoir is shown by the two-sided arrow.

The presented dependencies (Fig. 7) are calculated for thresholds of registration with increasing values from 3 to 6 MeV. Here it is very important to emphasize that registration with increasing threshold allows to decrease the count errors in order of values (in case of threshold rising from 3 to 6 MeV). This important result is explained by greater yield of ${}^8\text{Li}$ flux in the total $\bar{\nu}_e$ -flux (remembering that: the reactor spectrum is known with significant errors; the reactor spectrum drop rapidly as energy increases compare to well-known hard $\bar{\nu}_e$ -spectrum with mean energy ~ 6.5 MeV). The problems of errors lowering for $\bar{\nu}_e$ -spectrum and proposal to increase the threshold of $\bar{\nu}_e$ -registration are considered in details in [14–16]. The function of errors from the hardness H of the total spectrum was obtained (see in [14–16]).

4. CONCLUSION

The principle of the source operation is (n, γ) -activation of pure ${}^7\text{Li}$ near the reactor active zone and transfer of the activated lithium to remote detector by the loop scheme. The more perspective way of the source realization is to use the heavy water solution of ${}^7\text{Li}$ instead of metallic lithium [16–18] (taking in mind the requestion of ${}^7\text{Li}$ purification and price of very pure ${}^7\text{Li}$ (with grade of purification $\sim 99.99\%$ and higher) [16, 19].

Namely owing to cross section dependence $\sigma_\nu \sim E_\nu^2$ the number of neutrino interaction strongly increases at rise of the hardness (thanks to ${}^8\text{Li}$ neutrinos) of the total spectrum. High rate of the detector counts allows to use compact neutrino detector ($\sim \text{m}^3$).

Here it was considered the variant of the $\bar{\nu}_e$ source with realistic dimension and regime of operation. The possible scheme of the experiment for search of sterile neutrinos with $\Delta m^2 \sim 1 \text{ eV}^2$ is discussed for neutrino models (3+1) and (3+2). For this cases the total antineutrino fluxes were calculated taking into account both lithium and reactor spectra and corresponding errors, the dynamics of lithium transfer and dimensions of all parts of the installation. The oscillation probabilities for (3+1)-model and two variants of (3+2)-models

were simulated for different geometries of detector positions that allowed to indicate the space coordinates for search $\bar{\nu}_e$ -disappearance outside the spectrum errors.

Acknowledgements

We are grateful to L.B. Bezrukov, B.K. Lubsandorzhev, Yu.S. Lutostansky and I.I. Tkachev for stimulating discussions and support of the work.

The work is supported by the Russian Foundation for Basic Research Grants no.18-02-00670_a.

References

1. Schreckenbach K., Colvin G., Gelletly W. and von Feilitzsch F., *Determination of the anti-neutrino spectrum from ^{235}U thermal neutron fission products up to 9.5 MeV*, Phys. Lett. B., **160** (1985) 325.
2. Huber Patrick, *Determination of antineutrino spectra from nuclear reactors*, Phys. Rev. C., **84** (2011) 024617.
3. Kopeikin V.I., *Flux and spectrum of reactor antineutrinos*, Phys. At. Nucl., **75** (2012) 143–152.
4. Lyashuk V.I. and Lutostansky Yu.S., *Intensive neutrino source on the base of lithium converter*, (2015). arXiv:1503.01280v2.
5. An F.P. et al., (Daya Bay Collaboration), *Phys. Rev. Lett.* **116**. (2016) 061801.
6. Hayes A.C., Friar J.L., Garvey G.T., Ibeling Duligur, Jungman Gerard, Kawano T., Mills Robert W., *Possible Origins and Implications of the Shoulder in Reactor Neutrino Spectra*. (2015). arXiv:1506.00583v2 [nucl-th].
7. Huber Patrick, *Reactor antineutrino fluxes – status and challenges*.(2016). arXiv:1602.01499v1 [hep-ph].
8. Mikaelian L.A., Spivak P. E. and Tsinoev V.G., *A proposal for experiments in low-energy antineutrino physics*, Nucl. Phys. **70** (1965) 574–576.
9. Energy Levels of Light Nuclei $A = 8$, Nucl. Phys. **A745** (2004) 155.
10. Lyashuk V.I. and Lyutostansky Yu.S. *The conception of the powerful dynamic neutrino source with modifiable hard spectrum*. Preprint ITEP-38-97, Moscow: ITEP (1997); <https://lss.fnal.gov/archive/other/itep-38-97.pdf>
11. Lutostansky Yu.S. and Lyashuk V.I., *Powerful dynamical neutrino source with a hard spectrum*,/ Phys. Atom. Nucl. **63** (2000) 1288.
12. Lutostansky Yu.S. and Lyashuk V.I., *The concept of a powerful antineutrino source*,/ Bull. Russ. Acad. Sci. Phys. **75** (2011) 468.
13. Lyashuk V.I., *High ux lithium antineutrino source with variable hard spectrum*.(2017). [arXiv:1609.02934](https://arxiv.org/abs/1609.02934).
14. Lyashuk V.I., *Problem of reactor antineutrino spectrum errors and it's alternative solution in the regulated spectrum scheme*. Results Phys. **7** (2017) 1212.
15. Lyashuk V.I. (2018). arXiv:1809.05949.
16. Lyashuk V.I., *Intensive electron antineutrino source with well defined hard spectrum on the base of nuclear reactor and 8-lithium transfer. The promising experiment for sterile neutrinos search*, JHEP 06 (2019)135.
17. Lyutostansky Yu.S. and Lyashuk V.I., *Reactor neutrino-antineutrino converter on the basis of lithium compounds and their solutions*, Sov. J. At. Energ. **69** (1990) 696–699.
18. Lyashuk V.I., Lutostansky Yu.S. *Neutron sources for neutrino factory on the base of*

- lithium converter*, Proc. XXI Int. Seminar of Interaction of Neutrons with Nuclei. Alushta, May 20–25, 2013. Dubna, JINR, 2014, P. 156–164.
19. Lyashuk V.I., *Hard Antineutrino Source Based on a Lithium Blanket: A Version for the Accelerator Target*, Phys. Part. Nucl. Lett., **14** (2017) 465.
 20. <http://www.pnpi.spb.ru/en/facilities/reactor-pik>.
 21. Aksenov V.L., *Reactor PIK. Present status and trends*. Proceedings of Collaboration and Perspectives of Russian and Chinese Mega Projects, Dubna, Russia, December 3–4, 2014.
 22. LSND collaboration. *Evidence for neutrino oscillations from the observation of anti-neutrino(electron) appearance in a anti-neutrino(muon) beam*, Phys. Rev. D **64** (2001) 112007 [hep-ex/0104049].
 23. SAGE collaboration. *Measurement of the solar neutrino capture rate with gallium metal. III: Results for the 2002-2007 data-taking period*, Phys. Rev. C **80** (2009) 015807. [arXiv:0901.2200].
 24. MiniBooNE collaboration. *Event Excess in the MiniBooNE Search for $\bar{\nu}_\mu \rightarrow \bar{\nu}_e$ Oscillations*, Phys. Rev. Lett. **105** (2010) 181801 [arXiv:1007.1150].
 25. MiniBooNE collaboration. *Significant Excess of ElectronLike Events in the MiniBooNE Short-Baseline Neutrino Experiment*, Phys. Rev. Lett. **121** (2018) 221801. [arXiv:1805.12028].
 26. Giunti C. and Laveder M., *Statistical Significance of the Gallium Anomaly*, Phys. Rev. C **83** (2011) 065504 [arXiv:1006.3244].
 27. Mention G. et al., *The Reactor Antineutrino Anomaly*, Phys. Rev. D **83** (2011) 073006. [arXiv:1101.2755].
 28. Kopp J., Maltoni M. and Schwetz T. *Are there sterile neutrinos at the eV scale ?* Phys. Rev. Lett. **107** (2011) 091801 [arXiv:1103.4570].
 29. Maltoni M. and Schwetz T., *Sterile neutrino oscillations after first MiniBooNE results*, Phys. Rev. D **76** (2007) 093005 [arXiv:0705.0107].
 30. Conrad J.M., Ignarra C.M., Karagiorgi G., Shaevitz M.H. and Spitz J., *Sterile Neutrino Fits to Short Baseline Neutrino Oscillation Measurements*, Adv. High Energy Phys. **2013** (2013) 163897; [arXiv:1207.4765].
 31. Zysina N. Yu., Fomichev S.V. and Khruschov V.V., *Mass properties of active and sterile neutrinos in a phenomenological (3+1+2) model*, Phys. Atom. Nucl. **77** (2014) 890; [arXiv:1401.6306].
 32. Khruschov V.V., Fomichev, *Sterile neutrinos in uence on oscillation characteristics of active neutrinos at short distances in the generalized model of neutrino mixing*, Int. J. of Modern Physics A, **34**, No. 29 (2019) 1950175.
 33. KamLAND RCNS Group collaboration. *An overview of the KamLAND 1-kiloton liquid scintillator*. physics/0404071.
 34. Kopp J., Machado P.A.N., Maltoni M. and Schwetz T., *Sterile Neutrino Oscillations: The Global Picture*, JHEP 05 (2013) 050 [arXiv:1303.3011].